Computational study of microwave oscillations in nonstandard spin valves in the diffusive transport limit

E. Jaromirska,[1] P. Baláž,[2] L. López Díaz,[1] and J. Barnaś[2,3]
[1]*Departamento de Física Aplicada, Universidad de Salamanca, E-37008 Salamanca, Spain*
[2]*Department of Physics, Adam Mickiewicz University, Umultowska 85, 61-614 Poznań, Poland*
[3]*Institute of Molecular Physics, Polish Academy of Sciences, Smoluchowskiego 17, 60-179 Poznań, Poland*
(Received 15 June 2009; revised manuscript received 30 October 2009; published 11 January 2010)

An anomalous (inverse) spin accumulation in the nonmagnetic spacer may build up when the spin valve consists of magnetic films having different spin asymmetries and spin-diffusion lengths [J. Barnaś, A. Fert, M. Gmitra, I. Weymann, and V. K. Dugaev, Phys. Rev. B **72**, 024426 (2005)]. This leads to *wavylike* dependence of spin-transfer torque on the angle between magnetizations, as predicted by spin-dependent diffusive transport model, and also confirmed experimentally. Making use of these predictions, we have numerically studied the magnetization dynamics in the presence of such a wavy torque in Co(8 nm)/Cu(10 nm)/Py(8 nm) nanopillar, considering geometry with extended and etched Co layer. In both cases we specify conditions for the out-of-plane precession to appear in absence of external magnetic field and thermal fluctuations. We prove the assumption of wavylike torque angular dependence to be fully consistent with experimental observations. We also show that some features reported experimentally, such as nonlinear slope of frequency vs current, are beyond the applicability range of the macrospin approximation and can be explained only by full micromagnetic analysis.

DOI: 10.1103/PhysRevB.81.014408 PACS number(s): 75.60.Jk, 67.30.hj, 75.70.Cn, 78.20.Bh

I. INTRODUCTION

The concept of spin transfer was introduced in pioneering works by Slonczewski[1] and Berger.[2] They have shown that spin-polarized current can exert torque on a thin magnetic film due to transfer of spin angular momentum, which can influence magnetic state of the layer. The spin-transfer torque (STT) originates from spin asymmetries of the two independent transport channels, and its well-known manifestation is current-induced magnetic switching (CIMS) (Refs. 3 and 4) as well as generation of microwave oscillations.[5,6] Characteristics of STT are related to the sample design and material parameters. This also implies that CIMS and current-perpendicular-to-plane giant magnetoresistance (CPP-GMR) phenomena are correlated[7] and depend on the same structural parameters.

By considering two well-defined conduction spin channels, Valet and Fert[8] incorporated most of these parameters into CPP-GMR model based on spin-diffusion transport equations. Generalization of Valet-Fert approach[9] includes STT and provides an unified description of STT and CPP-GMR in the diffusive transport limit. For spin valves with fixed and free layer made of the same material, such as Co/Cu/Co, this model predicts standard behavior of STT, which does not vary qualitatively from Slonczewski's result obtained in the ballistic transport limit.[1] In this case, current of one orientation drives switching to antiparallel (AP) configuration while opposite current stabilizes parallel (P) state.[10] In presence of applied fields higher than the coercive field, the generation of microwave oscillations is possible.[6] Similar behavior has been recently observed also in Py/Cu/Py (Py=Permalloy), both experimentally[11,12] and theoretically.[13] Moreover, standard behavior of STT and the associated precession was also reported at high perpendicular magnetic field in an asymmetric spin valve,[14] where the magnetic layers are made of different materials [Co(40 nm)/Cu(10 nm)/Py(3 nm)]. However, a qualitatively different situation may arise in such asymmetric structures, where the spin asymmetries and spin-diffusion lengths differ markedly in both magnetic materials and the thicknesses obey certain conditions. The STT vanishes and changes sign in a certain noncollinear magnetic configuration (*wavylike* STT) due to the appearance of an inverse spin accumulation in the nonmagnetic spacer. Therefore, current flowing in one direction destabilizes both collinear magnetic configurations whereas the opposite current stabilizes both of them. The first case is of particular interest as it leads to excitation of stationary oscillation modes in absence of external magnetic field.[9]

In this paper we present a systematic study of dynamic response of a magnetic film to such wavylike STT. The asymmetric pillar under study consists of a fixed layer, nonmagnetic spacer, and a free magnetic layer; Co(8 nm)/Cu(10 nm)/Py(8 nm) spin valve with the elliptical cross section of 155×100 nm^2. The polarization of the fixed layer is assumed to be along the ellipse major axis. Recently, such asymmetric structures have been investigated theoretically[9,15,16] as well as experimentally at low and zero applied field.[17,18] To authors' best knowledge, no micromagnetic analysis of such structures in the diffusive transport limit has been performed so far. Moreover, the reported macrospin (referred to in the following also as single domain) study does not describe correctly the dynamics at low applied magnetic field.[18] Here, starting with the single-domain approximation, and extending study to the full micromagnetic model, we explain the origin of the out-of-plane precession (OPP). In particular, we show that only full micromagnetic model successfully reproduces magnetization dynamics at low applied magnetic field.

The paper is organized as follows. Section II describes briefly the torque calculations in the diffusive transport limit.

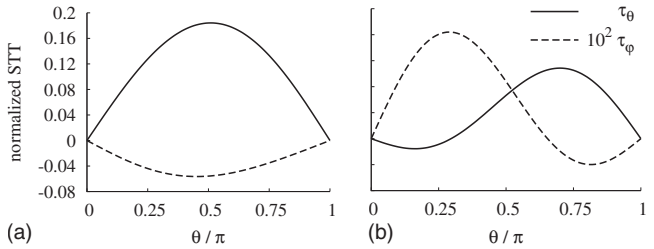

FIG. 1. Angular dependence of the spin-transfer torque normalized to $\hbar j/|e|$ for (a) symmetric Py(8 nm)/Cu(10 nm)/Py(8 nm) and (b) asymmetric Co(8 nm)/Cu(10 nm)/Py(8 nm) pillar. The parameters used in calculations are as follows: resistivity ($\mu\Omega$ cm), asymmetry factor, and spin-diffusion length (nm) for copper are 0.5, 0.0, and 1000, for cobalt 5.1, 0.51, and 60, and for permalloy 16, 0.77, and 5.5, respectively. The interfacial parameters: resistance ($f\Omega$ m^2), asymmetry factor, and real and imaginary parts of the mixing conductance ($1/f\Omega$ m^2) for the Co/Cu interface are 0.5, 0.77, 0.542, and 0.016, and for Py/Cu 0.5, 0.7, 0.39, and 0.012, respectively.

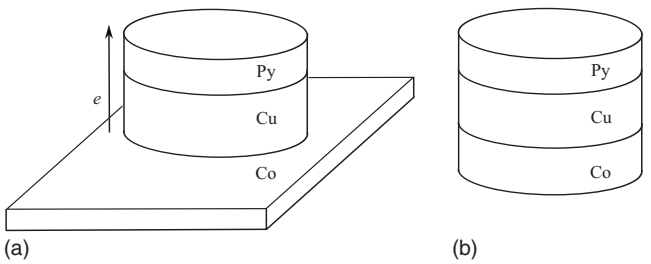

FIG. 2. Geometry of a pillar with (a) an extended and (b) etched fixed layer. The interlayer coupling field in (a) can be neglected.

The methodology of simulations is presented in Sec. III. The results of numeric study and their discussion are to be found in Sec. IV whereas final conclusions are in Sec. V.

II. SPIN TORQUE IN AN ASYMMETRIC PILLAR

As mentioned in Sec. I, structure of a pillar determines the dependence of STT on the angle between magnetization vectors. Generally, STT consists of two components, $\boldsymbol{\tau}=\boldsymbol{\tau}_\theta+\boldsymbol{\tau}_\varphi$, where $\boldsymbol{\tau}_\theta$ is the in-plane (IP) component while $\boldsymbol{\tau}_\varphi$ is the out-of-plane (OP) one. These two components can be written as[9]

$$\boldsymbol{\tau}_\theta = -aj\mathbf{m}\times(\mathbf{m}\times\mathbf{p}), \tag{1a}$$

$$\boldsymbol{\tau}_\varphi = bj\mathbf{m}\times\mathbf{p}, \tag{1b}$$

where $\mathbf{m}$ denotes the normalized (unit) vector along the magnetization of the free layer, $\mathbf{p}$ is the normalized magnetization of the fixed layer, and j is the current density. The prefactors a and b are independent of current j but they generally depend on the angle θ between $\mathbf{m}$ and $\mathbf{p}$. These parameters have been computed from the diffusive transport model[9] and fitted with cosine series for further numeric implementation, i.e., $a=a_0+a_1\cos(\theta)+a_2\cos^2(\theta)+a_3\cos^3(\theta)+a_4\cos^4(\theta)$ and analogously for b. In the first stage we use the diffusion spin equations and proper boundary conditions[19] to calculate the spin current. The torque is then calculated from the normal component of the spin current in the nonmagnetic film at the interface with the magnetic layer. Most of the parameters used in this description, such as interface and bulk spin asymmetry coefficients, interface resistances, layer resistivities,[20] and spin-diffusion lengths[21] are provided by the corresponding CPP-GMR experiments. The two remaining parameters, i.e., the real and imaginary parts of the mixing conductance[22] have been extracted from spin-current interface transmission calculations.[23] The variation in normalized (to $\hbar j/|e|$) STT with the angle θ for symmetric and asymmetric spin valves is shown in Fig. 1.

In the systems under considerations, the OP torque is roughly two orders of magnitude smaller than the IP component, which means that the former will not markedly influence the magnetization dynamics. Comparing the angular dependence for the standard [Fig. 1(a)] pillar structure with that for the nonstandard one [Fig. 1(b)], the uniqueness of the latter is clearly visible—at some critical angle θ the IP component of the torque vanishes. This gives rise to interesting dynamics at zero and low magnetic field. Above certain threshold current both collinear states of the magnetization are unstable for one current orientation, and the only solution of the Landau-Lifshitz-Gilbert (LLG) equation (within the macrospin model) is the steady-state precession or a noncollinear static magnetization state.[24]

Note also that the torque calculations are based on a one-dimensional transport model,[9] where the lateral diffusion was neglected. The model requirement of sample cylindrical symmetry is approximately fulfilled since in both structures presented in Fig. 2 any cross section can be treated as cylindrical symmetric, and thus change in pillar lateral dimensions does not affect the torque calculations. Accordingly, both an extended and etched pillar are characterized by the same torque shape.

III. SIMULATION METHODOLOGY

Magnetic dynamics of the free layer is described by the LLG equation with the STT included. This equation, when written as the equation for time evolution of the unit vector $\mathbf{m}$, takes the form

$$\frac{1+\alpha^2}{\gamma_0 M_S}\frac{d\mathbf{m}}{dt} = -\mathbf{m}\times\mathbf{h}_{\text{eff}} - \alpha\mathbf{m}\times(\mathbf{m}\times\mathbf{h}_{\text{eff}}) + \frac{j}{\mu_0 M_S^2 d}[\tilde{a}\mathbf{m}\times(\mathbf{m}\times\mathbf{p}) - \tilde{b}\mathbf{m}\times\mathbf{p}], \tag{2}$$

where $\tilde{a}=a-\alpha b$, $\tilde{b}=b+\alpha a$, $\mathbf{h}_{\text{eff}}$ is the effective field normalized to the saturation magnetization M_S of the free layer, α is the damping constant, d is the thickness of the free layer, and $\gamma_0=|\gamma|\mu_0$ with γ being the gyromagnetic ratio and μ_0 standing for the magnetic vacuum permeability. Since α is small, in following study we assumed $\tilde{a}=a$ and $\tilde{b}=b$.

In our convention the current flowing from the fixed toward the free layer defines the positive current direction, $j>0$. Note that in this convention the positive current triggers switching to the antiparallel configuration whereas negative current stabilizes parallel alignment in standard spin valves. On the other hand, negative current in nonstandard

spin valves supports oscillatory regime while positive current stabilizes both collinear configurations.

Only the dynamics of the free layer is resolved while magnetization of the fixed layer is assumed to remain uniform in the film plane. Neglecting the dynamics in the latter is justified by the experimental data. Boulle *et al.*[17] states that similar results were obtained for structures with the extended cobalt layer deposited directly on the electrode and for unetched cobalt layer additionally exchange biased by IrMn layer. This leads to the conclusion that the experimentally observed dynamics is localized in the free layer. Additionally, the fact that the saturation magnetization and anisotropy field are much larger in the cobalt (than in the permalloy) supports the assumption of this layer remaining fixed. Thus, in what follows we neglect its dynamics. Apart from this, we have neglected all thermal effects.

On the other hand, the Oersted field has been calculated in the infinite wire approximation, and its influence on dynamics has been taken into account. Using the micromagnetic spectral mapping technique[25–28](MSMT), we have determined the spatial localization of the modes when the Oersted field was added. The main excited mode is the uniform one, even if the Oersted field is incorporated. One should note that for the systems under study the the Oersted field is rather small as compared to the self-magnetostatic field, and therefore no significant changes neither in the frequency-current behavior nor mode spatial localization due to Oersted field have been reported, as expected. Thus, in the following systematic micromagnetic study this contribution has been neglected.

In the macrospin analysis, the effective field is assumed to include the self-magnetostatic term,[29] the uniaxial anisotropy field, and the external magnetic field. The uniform magnetostatic coupling field (with the fixed layer) is also taken into account. In the micromagnetic study, on the other hand, the magnetic field is modified with respect to macrospin case. First, the self-magnetostatic term is computed using the fast Fourier-transform technique assuming that the magnetization is uniform in each computational cell.[30] Second, six-neighbor dot-product representation is used to compute the exchange field. Unless stated differently in the text, the following values of the relevant parameters for permalloy have been chosen; the anisotropy constant $K_u = 3.46 \times 10^3$ J/m^3, exchange constant $A = 1.3 \times 10^{-11}$ J/m, damping constant $\alpha = 0.01$, saturation magnetization of Py $M_S = 6.9 \times 10^5$ A/m, and saturation magnetization of the fixed (Co) layer $M_{S\ \mathrm{fixed}} = 1.4 \times 10^6$ A/m. As follows from this choice, the corresponding exchange length $l_{\mathrm{exch}} = \sqrt{2A/\mu_0 M_S^2}$ equals 6.6 nm, and therefore we choose $5 \times 5 \times 4$ nm^3 discretization mesh. Further refinement of the cell size in the z direction does not lead to any substantial difference in system frequency response. Finally, the fourth-order Runge-Kutta scheme was employed for the time integration of Eq. (2), and the stability analysis was carried out for the chosen mesh to assign appropriate time integration step.

IV. RESULTS AND DISCUSSION

Before comparing results obtained from macrospin approximation with those from full micromagnetic study, one should consider that the concept of a single-domain magnetic particle in many situations is not justified. We shall explain how the difference between the results of macrospin and micromagnetic analyses arises from the appearance of an inhomogeneous magnetization and a finite exchange field. The exchange energy density of a closed $\boldsymbol{M}(\boldsymbol{r})$ configuration increases as the particle size decreases, and this could, in principle, justify macrospin approach below certain critical size of the system, even though spin torque makes the estimation of this critical size difficult.[31] However, as reported in Ref. 32, steady-state precession of a thin square nanoelement exhibits complicated transition from quasimacrospin to chaotic behavior already at the size of 30 nm, which invalidates single-domain approximation for most of experimentally studied systems. Moreover, on the basis of micromagnetic analysis Berkov and Gorn[33] identified some artifacts of the macrospin model in the ballistic transport limit. These artifacts might cause misleading interpretation of the origin of some observed phenomena, i.e., the frequency jumps observed in Ref. 6 were interpreted, within macrospin approximation, as a transition between small-angle and large-angle orbit motions while full micromagnetic study[33] revealed that the real origin of the jump was the loss of coherence and the appearance of quasichaotic regime. Being aware of that, we cannot, however, deny that macrospin dynamics is very rich and in many cases can serve as a tool for the basic understanding of physics behind.

Since the precessional states appear for negative current (according to the definition introduced in Sec. III), we limit the following considerations to this current direction only. For the sake of simplicity, in what follows the current I denotes the absolute value of the negative current.

A. Extended geometry

We start our numeric study with a pillar structure having an extended fixed layer, such as the one shown schematically in Fig. 2(a). The influence of the magnetostatic interlayer coupling field (ICF) can be then neglected. Since the anisotropy of Py is small, one also may conclude that it is mainly the self-magnetostatic field that drives the system dynamics.

In the following we will consider the role of initial magnetic state of the system. We start our considerations with the parallel initial magnetic configuration.

1. Initial P state

Assume the system is initially in the parallel magnetic configuration and increase the current stepwise (with the step ΔI) in order to identify possible oscillatory regimes. As the initial state for simulation at a given current $I + \Delta I$ we assume the state the system arrived at in the preceding step of simulations, i.e., for current I. Simulation results in both macrospin approximation and micromagnetic model reveal that an in-plane precession (IPP) is supported at zero applied field, which is consistent with previous analysis.[15,16] The associated frequency redshift with current is a well-known phenomenon and is attributed to the increase in the oscillation amplitude.[31] Interestingly, the redshift in the micromagnetic model turns out to be much smaller than in the macrospin

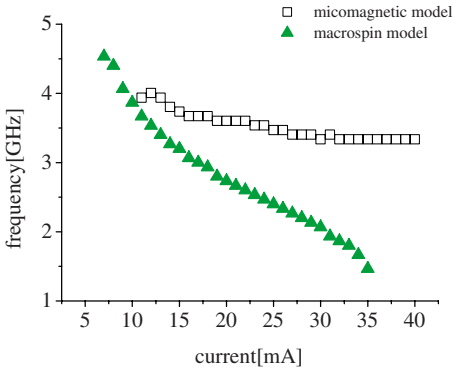

FIG. 3. (Color online) Frequency vs current in absence of external field in the macrospin model—full triangles and in the micromagnetic model—open squares. This convention is kept throughout this paper: open symbols correspond to results of micromagnetic study and full symbols to those in the macrospin model. A cutoff current is observed at $I=35$ mA in the single-domain model. The simulations have been performed for stepwise increasing current and for parallel initial magnetic configuration of the system. As the initial state for current $I+\Delta I$ we assume the state the system arrived at in the simulation step for the current I.

approximation, see Fig. 3, which is opposite to the results obtained in the ballistic transport limit.[31]

As follows from Fig. 3, the precessional states in the macrospin model disappear above a certain "cutoff" current ($I=35$ mA), where a stable static "spin-up" (normal to the film plane) magnetization state appears. Existence of this static state has been recently reported in Refs. 15, 34, and 35, where it was confirmed that the LLG equation has just two possible macrospin solutions—self-sustained precession or a stable static state. The appearance of the latter can be explained with the help of the diagram shown in Fig. 4. As the current is applied and the system is initially in the P state, the STT counterbalances the damping, and steady state IPP_+ (precession around $+x$ direction) is obtained in the region I. When the current is increased, the oscillation amplitude increases, and then the critical angle, (marked with the cross in Fig. 4) at which the torque vanishes, is reached. The magnetization starts then aligning along the effective magnetic field, and finally the stable spin-up state (circle in Fig. 4) is reached at the cutoff current. No such static state has been reported in micromagnetic simulations, where the redshifting branch is observed for currents well above 35 mA, see Fig. 3.

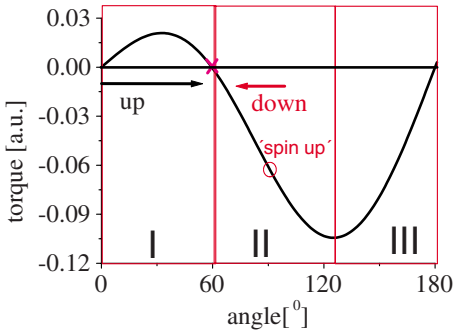

FIG. 4. (Color online) The torque normalized to $\hbar j/|e|$ for negative current density ($j<0$, compare Fig. 1) acting on the free layer. As the current is increased, the frequency redshift due to the amplitude increase is observed (angle θ increases, region I). When the critical angle is reached (cross between the regions I and II), the torque vanishes and the magnetization tends to align along the effective-field-driving system out of the critical angle toward the stable static spin-up state. The arrows indicate direction of current change.

Assume now that the system in the macrospin simulations reached the static spin-up state, and then the current is decreased (region II). The self-magnetostatic field and the STT may trigger now the OPP in a certain current range, as shown in Ref. 16. However, no OPP has been reported in the corresponding micromagnetic simulations.[36] Thus, even though single-domain model predicts the OPP mode, which was also reported experimentally,[18] the interpretation of its origin requires further considerations. This OPP mode will be obtained here in a different way, as shown and discussed below.

We have also checked the situation when current is increasing stepwise, with the initial P state at each simulation step. The results are equivalent to those presented in Fig. 3 for both micromagnetic and macrospin simulations.

2. Initial AP state

As we have seen above, two factors play a crucial role in the excitation of precessional states in the system. These are, the magnetization state, which imposes the initial self-magnetostatic field and the initial angle between the magnetic moments of the layers, which determines the initial torque sign and strength. The IPP_+ mode supported in the region I (Fig. 4) has been found in both macrospin and micromagnetic models whereas the static state in the region II has been found only in the macrospin approximation.

In order to investigate modes supported in region III, we have performed similar simulations but assumed AP configuration at the initial simulation stage. As before, we have analyzed two situations—when the final state at a given simulation step is assumed as the initial state in the next simulation step, and when the AP initial state was assumed at each simulation step. Consider first the former situation.

As the current is increased, the micromagnetic simulations reveal a fast redshifting branch in the range marked as 1 in Fig. 5 (open squares), corresponding to the IPP_- mode (precession around the $-x$ axis). Fast amplitude increase with increasing current leads to switching toward the P state and damped oscillations stabilizing the P state are observed (range 2). However, as certain threshold current ($I=7$ mA) is reached (P is now the initial state), the STT destabilizes the P state counterbalancing damping and the second redshifting branch, IPP_+, is observed (range 3). This branch is, thus, equivalent to the corresponding one in Fig. 3. Micromagnetically, the only difference between starting with initial P or AP state (open circles and open squares in Fig. 5, respectively) is the appearance of the first fast redshifting IPP_- branch.

Similar situation appears in the macrospin simulations. When we start from the AP initial state and increase current, we find the IPP_- mode (full squares in the region 1) and then the redshifting mode IPP_+ already seen in Fig. 3.

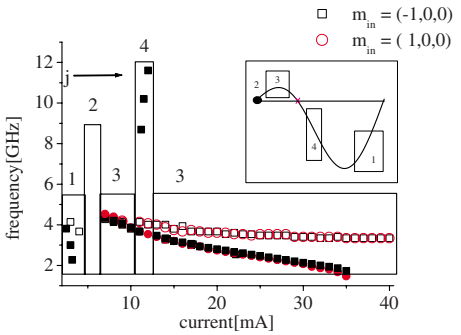

FIG. 5. (Color online) The influence of the initial magnetization state on the dynamic behavior of the system and the corresponding spots in torque diagram (inset). Circles refer to P whereas squares to AP initial state. At low currents, IPP_ mode (close to the AP direction) is found (marked as 1). As the current increases, the angle of the orbit increases as well, and $\langle m_x \rangle$ switches toward the P state. No self-sustained oscillations are observed in the range 2. Further current increase leads to the onset of the second redshifting branch, IPP_+, marked as range 3. Additionally at a certain threshold current, the combined effect of self-magnetostatic field of the AP initial state and negative torque sign can trigger the OPP in the macrospin model, marked as 4.

Consider now the case with the AP state assumed at each step of simulations (at each current step). As before, we find in the macrospin model both IPP_ and IPP_+ modes, except for the region 4 (full squares), where now a new mode is visible. This is the OPP mode, equivalent to that observed when starting simulation from the static point, as discussed above. Thus, if the current is large enough and the simulations are initialized with the AP state, the system might be forced to move into the region II (Fig. 4), leading to the appearance of OPP marked as range 4 in Fig. 5 (full squares).

Earlier in this section we have shown that after crossing from the region I through the critical angle into the region II, the static state can be observed. Here, though, dynamics in the region II is forced by the initial configuration and therefore the OPP can be observed. In other words, in the single-domain approximation the region I supports IPP_+ and region II supports static state or OPP (depending on the preceding configuration) whereas in region III the IPP_ mode can be observed. This result is consistent with the one reported in Ref. 15. However, no OPP mode was found in the micromagnetic simulations.

B. Etched geometry

In the etched geometry shown schematically in Fig. 2(b), the ICF can no longer be neglected. We have calculated this field micromagnetically, and neglecting large OP edge values we have estimated the average in-plane ICF to be −36 mT. This is a significant contribution and, therefore, dynamics different from that obtained for extended structures can be expected.

The dynamic response reveals now some new interesting features. To analyze them we have performed simulations for increasing as well as decreasing current. As the initial state for a particular simulation step we assumed the state reached

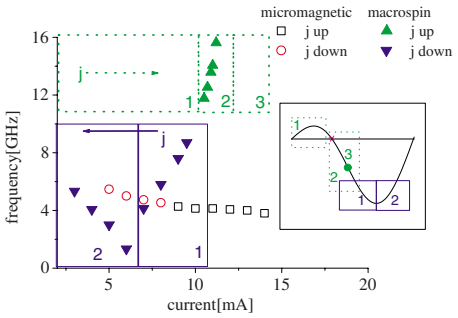

FIG. 6. (Color online) The influence of current increase and decrease in the etched pillar geometry on the dynamic response of the system with the initial P state. The corresponding torque diagram is shown in the inset. Note asymmetry in the macrospin frequency response—OPP with current increase and transition from OPP to IPP_ with current decrease are observed. This hysteretic behavior originates from the asymmetric torque angular variation and the existence of the critical angle making dynamic transition between the regions I and II of Fig. 4 prohibited.

in the preceding step. As before, the starting configuration (the first simulation step) was either P or AP state. Let us begin first with the P initial state.

1. Initial P state

Consider first macrospin analysis for increasing current. The initial P state leads now to the steady OPP, which appears at 10.4 mA when the current is increased, as indicated in Fig. 6 (see the upper part of the figure, with the corresponding range for the observed mode marked with dotted lines). As the threshold current for the OPP is reached, the blueshifting branch appears in the range 2. This OPP is not preceded by any IPP oscillations in the range 1 because the additional contribution from ICF places the system directly in region II (as defined in Fig. 4), i.e., the ICF favors AP configuration whereas the STT destabilizes it. As the frequency of the OPP mode increases with increasing current, the corresponding amplitude decreases and the angle between the magnetic moments of both layers approaches the critical angle. When this angle is reached, the static state discussed in the preceding section is observed (range 3). Let us now start decreasing current. The system is initially in the static point and dynamic range is marked with solid lines in Fig. 6 (bottom part). The OPP appears then in the corresponding range 1 at $I=9.8$ mA, and the amplitude and θ increase as the current decreases. The torque minimum is then passed and the system moves to the region III, which results in the appearance of the IPP_ mode in the range 2, where the amplitude decreases (with decreasing current), which results effectively in the frequency redshift with current. The asymmetry in the macrospin frequency response to increasing and decreasing current is clearly a consequence of the torque asymmetry, the existence of a critical angle, and irreversibility of the transition from region I to region II.

The dynamics in the micromagnetic model is simpler. Due to the effect of ICF, the system directly switches to the region III, and only one redshifting branch IPP_ is observed. A part of this branch is observed for increasing current and

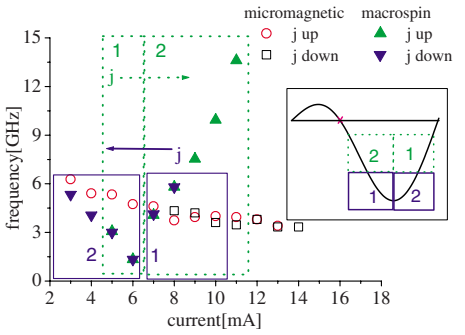

FIG. 7. (Color online) The same as in Fig. 6 but for the AP initial state. Micromagnetically only the IPP_ mode in the region III is observed.

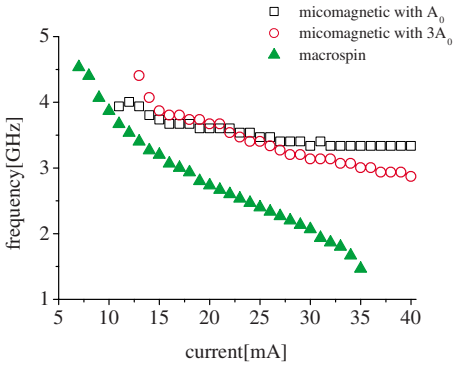

FIG. 8. (Color online) The dynamic response of the system for two different values of the exchange constant, compared to the macrospin results. Micromagnetically faster redshift is observed for larger exchange constant, as it favors more homogeneous magnetization configuration, i.e., more coherent dynamics.

the other part for decreasing current, as is clearly visible in Fig. 6. For decreasing current this mode is qualitatively similar to the macrospin mode observed in range 2.

2. Initial AP state

As discussed above, starting from the initial P state leads to a hysteretic dependence in the frequency response within the macrospin approximation. Consider now the situation with the initial AP state. When the current is increased (see the area bounded by the dotted line in Fig. 7), the system is directly placed in the region III, supporting redshifting branch (IPP_) in the range 1 (inset Fig. 7). As the amplitude increases with increasing current, transition to range 2, where the OPP mode is supported, is observed. In the torque diagram this is equivalent to the transition from region III over the torque minimum to the region II (Fig. 4). Since the critical angle is not crossed, this transition stays reversible and no hysteretic behavior in the frequency response is observed, i.e., both redshifting and blueshifting branches are observed for current being decreased and increased.

As before, no OPP was found in the micromagnetic simulations. For both increasing and decreasing currents only the IPP_ mode is observed. This indicates that the system supports stable oscillations only in the region III.

C. Influence of the exchange field

An open question is why the OPP modes obtained in the macrospin model and also reported experimentally,[18] have not been found in the micromagnetic simulations presented above. As it has been shown, to observe the OPP-associated blueshift, one has to force the system dynamics in the region II (Fig. 4). Moreover, we have learnt that the appearance of the macrospin spin-up state was a consequence of the crossing over the critical angle. This has not been reached micromagnetically due to the inhomogeneous nature of the magnetization (finite exchange field) in the model. Therefore, one should expect that the appearance of OPP in micromagentic model is hindered by the finite exchange field, and that increase in the exchange constant should lead to the convergence of both models. Using the bulk exchange constant for thin films might cause a significant underestimation of real exchange fields in these structures. Larger values of exchange constants, as compared to the standard bulk ones, have been reported in Py dots[37] and thin films.[38]

1. Extended geometry

In the extended geometry we have investigated magnetization dynamics for increasing current and for the following values of the exchange constant: $0.75A_0$, $2.5A_0$, and $3A_0$. The frequency-current behavior with $A=3A_0$ is compared to the results of macrospin model in Fig. 8. Clearly, increasing the exchange constant changes the slope of micromagnetic frequency redshift toward macrospin results. Thus, one may conclude that the finite exchange energy, favoring inhomogeneous magnetization state, drives less coherent dynamics and therefore causes this slope difference.

2. Etched geometry

In this geometry (ICF included) we have so far reported micromagnetically induced dynamics in the region III and the associated frequency redshift, as well as the macrospin dynamics in the region II supporting the OPP mode with the associated blueshift. Still, we want to check whether micromagnetic dynamics can be shifted to region II by increasing the exchange constant. The micromagnetic temporal evolution of the averaged magnetization at $I=13$ mA for $A=A_0$ and $A=2.5A_0$ results in different orbits, Figs. 9(a) and 9(b), respectively. Clearly in the first case the ICF places the sys-

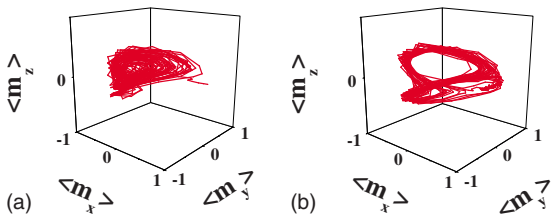

FIG. 9. (Color online) Visualization of the exchange constant influence on the magnetization dynamics in the etched geometry at $I=13$ mA. Magnetization orbit for (a) $A=A_0$ typical for the region III and (b) $A=2.5A_0$ approaching the border between regions III and II.

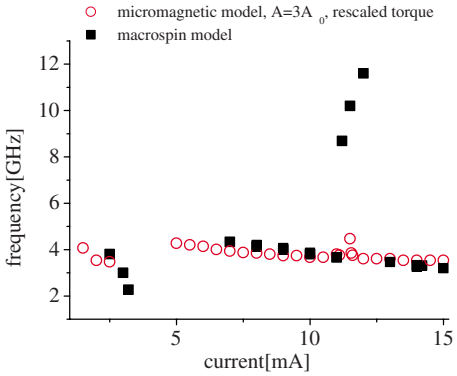

FIG. 10. (Color online) Comparison of the frequency vs current behavior at 0 mT for the macrospin and micromagnetic models with $A=3A_0$. As described in the text, in the micromagnetic model the torque strength has been scaled by a factor of 0.5 in order to counterbalance the effect of its inhomogeneous nature. The threshold for OPP predicted here by both models coincides with the experimental one (Ref. 18). The magnitude of the frequency jump associated with the transition IPP-OPP in the macrospin approximation does not fit the experimental values and micromagnetic approach proves to be more accurate.

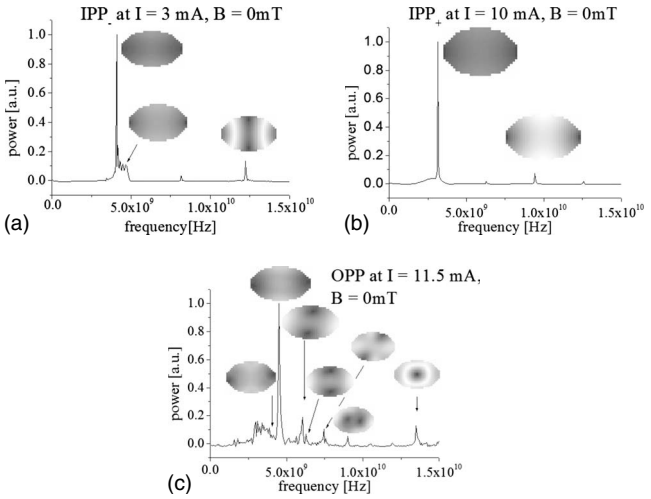

FIG. 11. The spectrum and power-density plots for (a) IPP_, (b) IPP_+, and (c) OPP modes. The main excited mode in all cases is the uniform mode. The IPP modes spectra exhibit some minor higher-order edge and hybrid modes whereas the spectrum of the OPP mode reveals the existence of various additional modes (hybrid, egde, and central modes).

tem in region III forcing IPP_ dynamics. However, as the exchange field is increased, which favors uniform magnetization, an open clamshell orbit is formed [Fig. 9(b)] shifting the dynamics toward the border between the regions III and II. One should note that the crossover between the regions is impossible in this geometry as the ICF has a significant impact on the effective field hindering the appearance of OPP mode.

D. Comparison to experimental data

So far no OPP (supported in the dynamic region II) has been predicted micromagnetically, even though such modes were reported experimentally[18] in extended structures. However, previous paragraphs have given some important clues. We have learnt about the importance of the exchange field. We assume $A=3A_0$ for further study. Second, as the magnetization always stays inhomogeneous to some extend, the torque calculated locally (cell by cell) inherits this inhomogeneity and we shall scale the torque strength by a factor of 0.5 to counterbalance this effect. Third, micromagnetically the transition from dynamic regions I to II was impossible. Thus, in order to observe the OPP, one has to force dynamics in the region II by forcing the transition from regions III to II (i.e., imposing the AP initial state). As presented in Fig. 10, indeed under all above-mentioned assumptions both models converge. Micromagnetic dynamics is forced first in the region III supporting IPP_, then switching toward P state takes place (range of current where no sustained oscillations are observed, as discussed before), and then IPP_+ branch (region I) is triggered. At certain threshold, however, the dynamics in region II supporting blueshift can be obtained. The threshold of this OPP coincides with the experimental one from.[18] The frequency gap associated with the transition IPP-OPP in the macrospin approximation does not fit to the experimental observations, i.e., according to macrospin data at 12 mA the frequency reaches 11.6 GHz and experimentally frequencies not higher than 4 GHz were reported. Micromagnetic approach proves to be more accurate, as no such gap is observed and the OPP mode frequency around 4 GHz is in agreement with the measured one. The origin of this discrepancy is linked to the fact that the macrospin precession takes place around the self-magnetostatic field axis[36] whereas in the real systems there are other contributions to the effective field, mainly the exchange field, which is beyond single-domain appoximation. Micromagnetic model not only incorporates this factor but also treating the system as continuum accounts for the inhomogeneous character of the effective field counterbalancing above-mentioned effect and thus, no frequency gap is observed in the IPP-OPP transition.

Summarizing, the micromagnetic dynamics in all three regions have been reported. Moreover, the redshift was identified as the IPP_ and the IPP_+ mode whereas the blueshift as the OPP mode. Employing the previously mentioned MSMT,[25–28] we have investigated the spatial profile of these modes. Monitoring the temporal evolution of the magnetization vector field allows, in the frames of MSMT, for determination of the spatial character of each peak in the spectral diagram. As presented in Fig. 11(a), the main peak in IPP_ spectrum corresponds to the uniform mode. Additionally a side peak representing another uniform mode is visible together with higher-order mode exhibiting hybrid spatial character. The modal analysis of the IPP_+ is even simpler revealing high-power uniform mode and a weak edge mode associated with a minor peak, as shown in Fig. 11(b). In both cases, the magnetization changes uniformly across the sample, giving rise to one dominant peak.

The spectrum representing the OPP [Fig. 11(c)] is more complicated. One should consider that the magnetization precessing out-of-plane looses partly its coherence.[31] Therefore, even though the main and dominant mode remains uniform, it is preceded by a quasiuniform mode and followed by

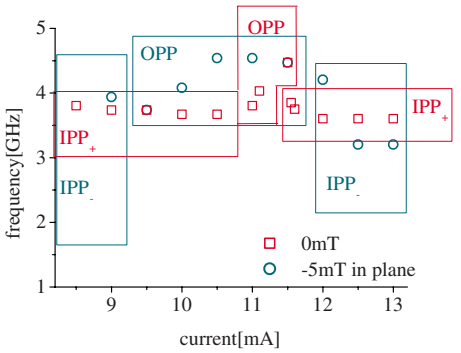

FIG. 12. (Color online) Results of micromagnetic model at zero and low applied field. The dynamic response at 0 and −5 mT applied in plane. In absence of external field IPP_+ transition into OPP at 10.5 mA and back to IPP_+ above 11.5 mA is observed. At −5 mT the transitions from IPP_- to OPP and back to IPP_- are observed at 9.5 and 12 mA, respectively. Both, blueshift linear at 0 mT and nonlinear at −5 mT predicted micromagnetically, are consistent with the experimental results (Ref. 18). Macrospin ceases to show the saturation regime observed experimentally at −5 mT but full micromagnetic study correctly predict this feature.

numerous edge and hybrid modes. In the picture of an evolving magnetization vector field, these modes simply correspond to the rotation being triggered in different parts of the sample. Moreover, at around 12.5 GHz an additional peak is observed. The magnetization in the central region of the sample tends to oscillate uniformly, giving rise to this extra central mode. Even though most of the power is emitted by the predominant uniform mode, the appearance of these side modes indicates that additional nonuniformities, such as the Oersted field, could suppress the main mode favoring more complicated modal structures. Still, since the frequency of the predominant mode is hardly influenced by the Oersted field, and its impact on the mode spatial localization is beyond the interest of this work, we simply neglect this contribution.

The fact that experimentally the OPP was reported by starting from P state (opposite to our results) means that transition between the regions I and II prohibited micromagnetically is experimentally possible due to thermal activation. As our simulations neglect the effect of temperature, the dynamic region II can be only reached by transition from region III. One should note that not all regimes (dynamics in all regions I, II, and III) predicted by the simulations for the extended geometry were observed experimentally. Low-angle IPP does not provide enough output power to be measured via GMR effect. Therefore, in order to conduct meaningful comparison we have concentrated on the OPP regime (region II), which was both predicted numerically and observed experimentally. In the absence of external field a satisfactory qualitative agreement has been reached (Fig. 12, compare to Fig. 6a in Ref. 18). Not only the threshold current ($I_{th,sim}$=11 mA compared to $I_{th,exp}$=10 mA) but also the agility (0.6 and 0.7 GHz/mA, respectively) are in good agreement. The remaining quantitative difference in frequency values is a consequence of uncertain estimation of the factors entering micromagnetic model, such as saturation magnetization and/or damping.

Moreover, the dynamics at −5 mT IP field reveals that OPP threshold current is smaller with respect to 0 mT case, which is again consistent with the experimental results. Interestingly, both approximately linear at 0 mT and nonlinear at −5 mT behavior of the frequency as a function of current, are well reproduced in frames of micromagnetic model. Note that this feature was not reported within single-domain approximation. Furthermore, micromagnetic model predicts experimentally observed saturation at −5 mT, i.e., in a certain current range the frequency stays relatively constant. In the model it is associated with the large-angle orbit stabilization around the torque minimum, i.e., the system approaches the border of dynamic regions II and III, and the torque shape becomes flat around its minimum. Current increase leads to transition between OPP (region II) and IPP_- (region III) and reappearance of the clamshell orbit. However, since neither was the IPP reported in the experiment prior to the appearance of OPP, as predicted micromagnetically, nor it could have been detected following OPP regime (because of low output power) so obviously the experimental cutoff current refers to the threshold current for IPP reappearance in the model. Note that micromagnetically the main mode (supported over largest range of currents) in case of 0 mT was the IPP_+ whereas even low applied field of −5 mT IP forced the dynamics in region III and, therefore, the IPP_- was observed as the main mode. In other words direct dynamics in region II in absence of external field (and associated linear frequency vs current slope) is favored by sufficiently high exchange field and additional external field forced the transition from region III to region II resulting in the appearance of the saturation regime. Clearly the OPP in both cases is preceded by different dynamics.

V. CONCLUSIONS

We have studied current-induced magnetic dynamics in spin valves within both macrospin and micromagnetic models. The results emerging from both models very often do not converge and are qualitatively different. We have shown how the discrepancies arise mainly from the inhomogeneous magnetization state and finite exchange field.

In the case of spin valves with nonstandard angular variation in spin torque, we have found that the OPP mode might appear in the macrospin model as a consequence of the spin-up static state. The static state seems to be a characteristic feature of such spin valves in the macrospin description.

In turn, the absence of OPP in the micromagnetic model was identified as a consequence of the underestimation of the exchange constant and the role of the initial self-magnetostatic field. By setting proper initial state and the exchange constant favoring the appearance of the OPP, a good qualitative agreement was reached between the predictions of both models. Thus, only full micromagnetic model has predicted correctly dynamics reported experimentally, i.e., quantitatively the frequency values as well as qualitative features such as the nonlinear frequency blueshift with current and the appearance of saturation regime at low applied field.

ACKNOWLEDGMENTS

This work was supported by EU Training Network SPINSWITCH (Grant No. MRTN-CT-2006-035327), Spanish goverment project MAT2008-04706/NAN, and Junta de Castilla y Leon project SA 025A08. Fruitful discussions with Luis Torres are also acknowledged. J.B. acknowledges support by funds from the Ministry of Science and Higher Education as a research project in years 2006-2009 within the EUROCORES Programme FoNE (project SPINTRA). P.B. acknowledges discussions with M. Gmitra.

[1] J. C. Slonczewski, J. Magn. Magn. Mater. **159**, L1 (1996).
[2] L. Berger, Phys. Rev. B **54**, 9353 (1996).
[3] M. AlHajDarwish, H. Kurt, S. Urazhdin, A. Fert, R. Loloee, W. P. Pratt, and J. Bass, Phys. Rev. Lett. **93**, 157203 (2004).
[4] M. Tsoi, J. Z. Sun, M. J. Rooks, R. H. Koch, and S. S. P. Parkin, Phys. Rev. B **69**, 100406(R) (2004).
[5] A. N. Slavin and V. S. Tiberkevich, Phys. Rev. B **72**, 094428 (2005).
[6] S. I. Kiselev, J. C. Sankey, I. N. Krivorotov, N. C. Emley, R. J. Schoelekopf, R. A. Buhrman, and D. C. Ralph, Nature (London) **425**, 380 (2003).
[7] M. Gmitra and J. Barnaś, Phys. Rev. B **79**, 012403 (2009).
[8] T. Valet and A. Fert, Phys. Rev. B **48**, 7099 (1993).
[9] J. Barnaś, A. Fert, M. Gmitra, I. Weymann, and V. K. Dugaev, Phys. Rev. B **72**, 024426 (2005).
[10] J. A. Katine, F. J. Albert, R. A. Buhrman, E. B. Myers, and D. C. Ralph, Phys. Rev. Lett. **84**, 3149 (2000).
[11] I. N. Krivorotov, N. C. Emley, J. C. Sankey, S. I. Kiselev, D. C. Ralph, and R. A. Buhrman, Science **307**, 228 (2005).
[12] I. N. Krivorotov, N. C. Emley, R. A. Buhrman, and D. C. Ralph, Phys. Rev. B **77**, 054440 (2008).
[13] I. N. Krivorotov, D. V. Berkov, N. L. Gorn, N. C. Emley, J. C. Sankey, D. C. Ralph, and R. A. Buhrman, Phys. Rev. B **76**, 024418 (2007).
[14] S. I. Kiselev, J. C. Sankey, I. N. Krivorotov, N. C. Emley, M. Rinkoski, C. Perez, R. A. Buhrman, and D. C. Ralph, Phys. Rev. Lett. **93**, 036601 (2004).
[15] M. Gmitra and J. Barnaś, Appl. Phys. Lett. **89**, 223121 (2006).
[16] M. Gmitra and J. Barnaś, Phys. Rev. Lett. **99**, 097205 (2007).
[17] O. Boulle, V. Cros, J. Grollier, L. G. Pereira, C. Deranlot, F. Petroff, G. Faini, J. Barnaś, and A. Fert, Nat. Phys. **3**, 492 (2007).
[18] O. Boulle, V. Cros, J. Grollier, L. G. Pereira, C. Deranlot, F. Petroff, G. Faini, J. Barnaś, and A. Fert, Phys. Rev. B **77**, 174403 (2008).
[19] A. Brataas, Yu. V. Nazarov, and G. E. W. Bauer, Eur. Phys. J. B **22**, 99 (2001).
[20] J. Bass and W. P. Pratt, Jr., J. Magn. Magn. Mater. **200**, 274 (1999).
[21] J. Bass and W. P. Pratt, Jr., J. Phys.: Condens. Matter **19**, 183201 (2007).
[22] A. Brataas, G. E. W. Bauer, and P. J. Kelly, Phys. Rep. **427**, 157 (2006).
[23] M. D. Stiles and A. Zangwill, J. Appl. Phys. **91**, 6812 (2002).
[24] J. Barnaś, A. Fert, M. Gmitra, I. Weymann, and V. Dugaev, Mater. Sci. Eng. B **126**, 271 (2006).
[25] R. D. McMichael and M. D. Stiles. J. Appl. Phys. **97**, 10J901 2005.
[26] M. Grimsditch, G. K. Leaf, H. G. Kaper, D. A. Karpeev, and R. E. Camley, Phys. Rev. B **69**, 174428 (2004).
[27] L. Torres, G. Finocchio, L. López Díaz, E. Martinez, M. Carpentineri, G. Consolo, and B. Azzerboni. J. Appl. Phys. **101**, 09A502 (2007).
[28] L. Torres, L. López Díaz, E. Martinez, G. Finocchio, M. Carpentineri, and B. Azzerboni, J. Appl. Phys. **101**, 053914 (2007).
[29] A. Aharoni, J. Appl. Phys. **83**, 3432 (1998).
[30] A. J. Newell, W. Williams, and D. J. Dunlop. J. Geophys. Res. **98**, 9533 (1993).
[31] D. V. Berkov and J. Miltat, J. Magn. Magn. Mater. **320**, 1238 (2008).
[32] D. Berkov and N. Gorn, Phys. Rev. B **71**, 052403 (2005).
[33] D. V. Berkov and N. L. Gorn, Phys. Rev. B **72**, 094401 (2005).
[34] P. Baláž, M. Gmitra, and J. Barnaś, Phys. Rev. B **79**, 144301 (2009).
[35] P. Baláž, M. Gmitra, and J. Barnaś, Acta Phys. Pol. A **115**, 278 (2009).
[36] E. Jaromirska, P. Baláž, L. López Díaz, and J. Barnaś, J. Appl. Phys. **106**, 113909 (2009).
[37] Z. H. Wei, M. F. Lai, Ch. R. Chang, N. A. Usov, J. C. Wu, and J. Y. Lai, J. Magn. Magn. Mater. **282**, 11 (2004).
[38] D. Scholl, M. Donath, D. Mauri, E. Kay, J. Mathon, R. B. Muniz, and H. C. Siegmann, Phys. Rev. B **43**, 13309 (1991).